HiSST: 3rd International Conference on
High-Speed Vehicle Science Technology
14 -19 April 2024, Busan, Korea

Assessment of Uranus planetary entry conditions in the X2 Expansion Tube for performing Infrared Thermography

Matthew Uren[1], Yu Liu[2], Chris James[3], Richard Morgan[4]

Abstract

A dedicated exploration mission of the ice giant planets has been prioritized as a key scientific objective by NASA and ESA to further understanding of their formation and atmospheric structure. In-situ measurements of the planetary atmosphere for giant planets has been successfully demonstrated with the Jupiter Galileo probe, however, there are significant uncertainties surrounding thermal loading and peak heating during giant planet entry. The usage of impulse ground test facilities, such as shock tunnels and expansion tubes, allows for the experimental simulation of planetary entry aerothermodynamics where such uncertainties can be investigated. Over the past decade, substantial development has gone into generating giant planet entry conditions at The University of Queensland's Centre for Hypersonics. Therefore, this work details the characterisation and assessment of Uranus peak heating entry conditions in the X2 expansion tube, and the suitability of the conditions for performing infrared thermography to obtain experimental heat flux data. Three test conditions were generated using the hypersonic facility analysis code PITOT3 and experimentally assessed in the X2 expansion tube using a Pitot pressure probe rake, a small fibre-coupled spectrometer, and a photodiode. Two of the conditions showed good repeatability across shots by assessment of the time-resolved Pitot pressure and photodiode measurements. Post shock properties were derived via PITOT3 using the experimental pressure measurements and an analytical thermal analysis was performed to predict the stagnation-point heat flux and subsequent surface temperature rise of a graphite test model. The convective heat flux calculations agreed well with predictions of ice giant entry heat flux from the literature and the surface temperature rise compared favourably to previous infrared thermography experiments in the X2 expansion tube. Whilst the test conditions appear suitable for the investigation of the Uranus peak heating trajectory point, the success of future experiments is dependent on the identification of a suitable waveband in the visible to IR spectrum and appropriate selection of temporal and spatial resolution over the test flow and model, and this will be the prime focus of future work towards obtaining experimental heat flux data.

Keywords: Ice Giant, Infrared Thermography, Expansion Tube, Shock Tunnel, Heat Flux

[1] *Centre for Hypersonics, School of Mechanical and Mining Engineering, The University of Queensland, St Lucia, QLD, 4072, Australia, matthew.uren@uq.edu.au*
[2] *Centre for Hypersonics, School of Mechanical and Mining Engineering, The University of Queensland, St Lucia, QLD, 4072, Australia, yu.liu1@uq.edu.au*
[3] *Centre for Hypersonics, School of Mechanical and Mining Engineering, The University of Queensland, St Lucia, QLD, 4072, Australia, c.james4@uq.edu.au*
[4] *Centre for Hypersonics, School of Mechanical and Mining Engineering, The University of Queensland, St Lucia, QLD, 4072, Australia, r.morgan@uq.edu.au*

1. Introduction

The ice giant planets, Uranus and Neptune, are the two least explored planets in our solar system. The formation and atmospheric structure of ice giant planets are currently not well understood, yet they are exceedingly common in observations of exoplanets in our galaxy. For these reasons, NASA and ESA have both prioritized the planning and development of an Orbiter and Probe mission to either Uranus or Neptune, with the scientific aim of further understanding the atmospheric structure of each planet [1-2].

Available data regarding the atmospheric structure of the two planets have largely been collected from the Voyager 2 mission fly-by's in the 1980's and any remaining data is due to observations made from Earth, as no dedicated ice giant probe mission has ever been flown. Therefore, the design of an entry probe for either planet is of interest to collect in-situ measurements of the atmospheric composition, pressure, and temperature during the entry trajectory. The mass budget for interplanetary probes can be largely dependent on the requirements of the thermal protection system, which is driven by the predicted thermal loading during entry. There are significant uncertainties in the prediction of surface heat flux for giant planet entry, and this depends largely on the non-equilibrium thermochemical phenomena in the shock layer and at the surface of the entry vehicle [3]. Therefore, understanding the mechanisms leading to surface heating during entry is crucial for the optimization and survivability of future giant planet probe missions.

Previous experience in giant planet mission entry can be drawn from the Jupiter Galileo probe mission in the 1990's, where in-situ measurements of the atmosphere were taken by the probe during entry. The recession of the Galileo probe heat shield differed from predictions, suggesting further understanding of the heating mechanisms of giant planet entry vehicles is required, however, there have not been any similar missions since Galileo and the original facility used to simulate these flows has since shut down [4]. The heating mechanisms for the giant planets are also vastly different, with radiative heating being the primary contributors for Jupiter, convective heating for Uranus, and both heating mechanisms for Saturn and Neptune [4-6].

Computational methods are often used for numerically solving the flow field and thermal loading, but they require validation and comparisons with experimental data to increase confidence in their predictions. Current methods to experimentally simulate giant planet entry flows consist largely of arc-jet facilities and high enthalpy expansion tubes. Arc-jets can provide long-duration high temperature environments for assessing material response; however, they cannot recreate a representative aerodynamic flow field nor high stagnation pressure**.** Contrastingly, high enthalpy expansion tubes can provide flight representative enthalpies and stagnation pressures with appropriately scaled shock layers for studying the non-equilibrium thermochemical processes unique to hypersonic entry flows. Although, the short test times on the order of 10s of micro to milliseconds make obtaining suitable data for investigating giant planet entry flows challenging.

Initial research in the early 2000's by Higgins [7], Inger [8], and Herbrig [9] established the feasibility of generating and studying aerothermodynamic flows representative of giant planet entry in the X2 expansion tube, a high enthalpy impulse ground test facility at The University of Queensland. These early efforts were built on substantially over the past decade by James [10-12] and Liu [13-14], opening a new avenue in higher enthalpy test conditions and radiative measurements. The recent interest in a mission to either Uranus or Neptune have prompted the need to study surface heating for ice giant entry conditions, particularly due to uncertainties in the surface chemistry and contributions to heating by radiation [4]. Shock layer radiation for ice giant planetary entry is suspected to be driven by trace elements of CH_4 in the atmosphere, in the order of 1.5%, and this has been experimentally studied for both Uranus and Neptune entry [15],[16],[17]. However, there are still outstanding questions regarding how the concentration of trace species such as CH_4 vary with altitude. Surface heating for ice giant representative test flows has been studied in the Oxford T6 Stalker Tunnel and the Stuttgart PWK1, via surface mounted coaxial thermocouples and heat flux

sensors, respectively [16,18]. However, the convective heat flux for ice giant entry has been shown to vary significantly dependent on the catalytic recombination of surface adsorbed gas species [4]. Therefore, the usage of surface mounted instrumentation restricts insights regarding catalytic activity to the sensor material, and this may not be truly representative of an entry vehicle heat shield.

Infrared Thermography (IRT) is a possible avenue for investigating the surface heat fluxes and catalytic recombination for ice giant representative test conditions in X2. IRT is a non-intrusive and spatially resolved heat flux measurement technique that has been demonstrated successfully in previous work on X2 [14-15]. The successful application of IRT requires an adequate signal-noise ratio, where the signal is the radiation from the test model surface, and the noise can be from radiation in the shock layer surrounding the test model. Significant radiation is not expected for Uranus entry due to the high ionization energies of hydrogen relative to that of the total flow enthalpy, however, contamination from the experimental facility could impede the successful application of IRT if it radiates significantly during the test time. This paper will firstly assess the capability of X2 to produce the test flow environments representative of Uranus peak heating, by assessment of the steady flow test time, Pitot rake pressure measurements, and the spatial variation of the core test flow. Secondly, analytical solutions for predicting surface heat flux will be used in combination with the assessed flow conditions to predict whether a sufficient surface temperature rise can be generated for adequate IR thermographic measurements. Future experiments are planned to take spectroscopic measurements across the UV, visible, and IR wavebands of the shock layer over a blunt body test model, and this will finalise the assessment of the suitability of the test conditions for performing Infrared Thermography on probe heat shield representative test models.

2. Experimental methodology

The X2 expansion tube is a free-piston-driven impulse facility currently used by The University of Queensland's Centre for Hypersonics to experimentally study hypersonic flight and planetary entry. The facility consists of a driver section with a gas compressing free piston, a driven shock tube section that houses the test gas for the experiment, and a low-pressure acceleration tube, as shown in Fig. 1. Prior to an experiment, the tunnel is pumped down to low pressures of 1-20 Pa and then filled with the required test gas compositions. The compression of the driver gas from the free-motion piston ruptures the primary diaphragm, driving a shock wave through the test gas, and the subsequent rupturing of the secondary diaphragm allows the shock heated test gas to unsteadily expand to higher enthalpies downstream towards the test section. Further details on the operation of the X2 expansion tube can be seen in [21]. Prior to the commencement of the testing campaign and due to the difficulty of achieving sub 5 Pa acceleration tube pressure, significant effort was made to identify and fix potential leak paths around the test section, driven tubes, and filling station manifolds. This was achieved via usage of a helium leak detector and identified leaks were addressed by the replacement of seals and the application of RTV.

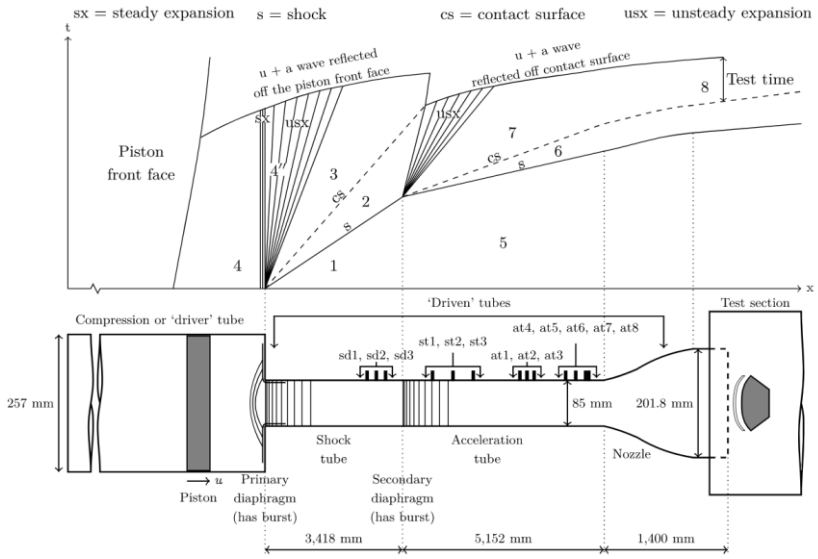

Fig. 1 X2 x-t diagram and layout

To characterise the generated flow conditions, a series of 112A ICP pressure transducers implemented into a one-dimensional array of Pitot probes as a Pitot rake was installed into the test section of X2, for assessment of the steady test time, core flow size, and mean flow pressure. The experimental set up of this can be seen in Fig. 2, where the Pitot probes are designated Pt1 to Pt9, from top to bottom, and the central probe Pt5 is aligned to the central axis of the test section nozzle. The positioning of the rake is chosen to ensure symmetry in the measured pressure about the central probe. Prior to commencement of the ice giant characterisation shots, a series of Earth re-entry Zander condition shots [22] were carried out to ensure the Pitot rake was performing as expected. Several pressure transducers were swapped out and the adjustment of the tightness of the pitot probe heads covering the transducers was required.

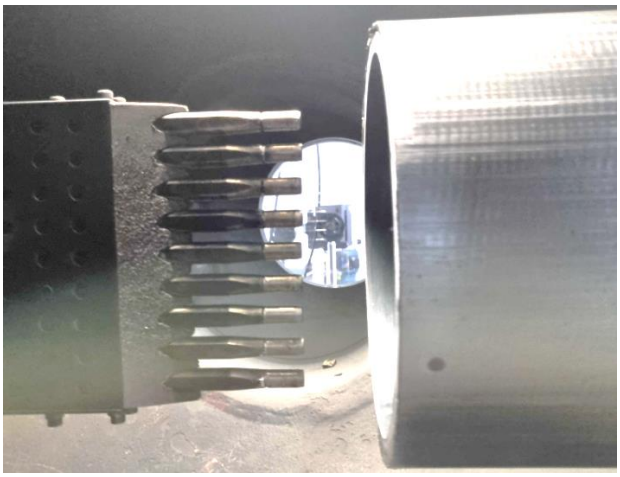

Fig. 2 X2 Pitot Rake

Analysis of the test flow and pressure measurements were performed using in-house codes Shot Class [23] and PITOT3 [24], the latter of which was used to derive freestream and post shock equilibrium flow properties of the test flow, based on the experimental shock speeds and Pitot pressure measurements. Optical measurements were made of the test flow over the pitot rake using a Shimadzu HPV-1 high speed camera with a H-alpha filter centered at 656 nm, a Thorlabs Compact CCD small fibre-coupled spectrometer to capture time-integrated signals of chemical species in the flow with intensities between 200 nm – 1000 nm, and a series of photodiodes sensitive between 350 nm – 2600 nm. Post-processing of the high-speed video data showed the signal strength after the initial shock arrival was too low to perform steady test time assessment, based on the integrated intensity of the flow over each probe during the test time. Therefore, the steady flow test time analysis was performed using a combination of visual assessment of the time-resolved pressure measurements in combination with photodiode measurements of probe number Pt7 on the rake. An example of the resultant steady test time regions identified according to Pitot probe pairs is shown in Fig. 3 by the dashed vertical lines indicating start and end of the test time. During the experimental data analysis, a time lag in startup for the outer probes relative to the central three was noticed which led to a trade-off in the selection of steady flow test time and core flow size. To address this, the steady test time regions for probe pairs {4,5,6}, {3 and 7}, and {2 and 8}, were assessed separately, and the resultant crossover in test time for the three groups was chosen to be the final steady test time for each condition. The condition shown in Fig. 3, for example, would obtain a steady test time between 75 μs and 125 μs, with a total test time of 50 μs.

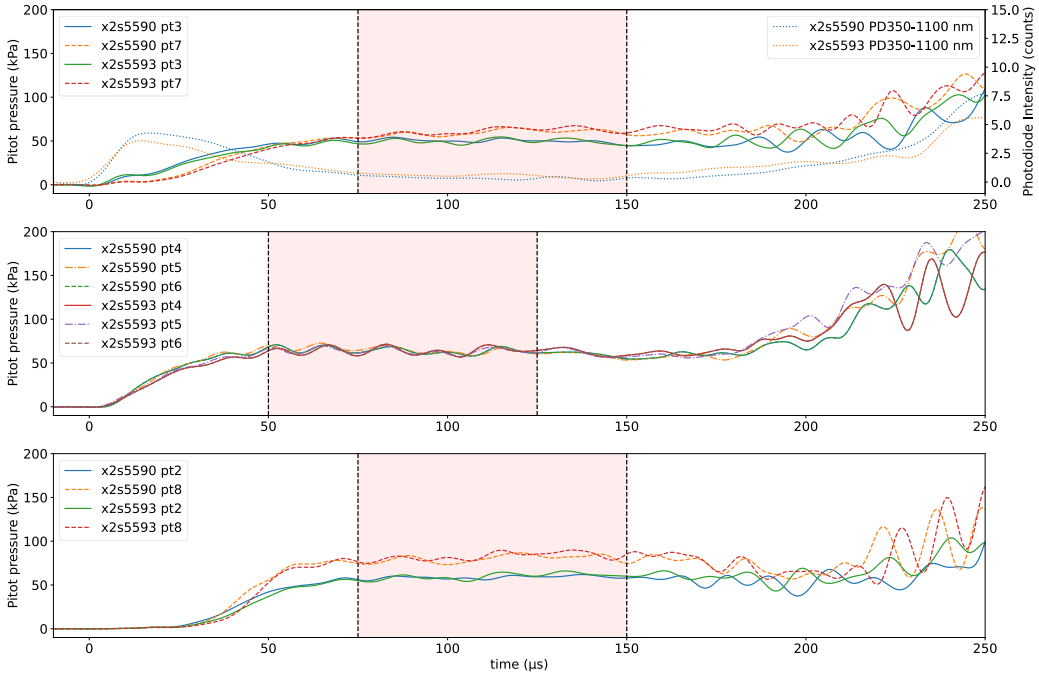

Fig. 3 Pitot pressure traces from shots x2s5590 and x2s5593

3. Experimental results

Using PITOT3 in condition builder mode, a sweep of theoretical X2 operating conditions for different fill pressures and compositions of hydrogen/helium was performed. The target condition was the Uranus peak heating equilibrium trajectory point discussed in [4], and the freestream and equilibrium post shock flow quantities for that trajectory point are shown in Tables 2 and 3, respectively. From the PITOT3 condition builder results, three possible conditions were chosen with different test gas compositions, and they are shown in Table 1. Test gas substitution by increasing the helium diluent in the test gas was implemented to enable matching of the target post shock temperature of ~4600 K at lower test flow velocities than the predicted real flight velocity. The additional helium increases the density of the test gas mixture whilst reducing the specific heat capacity of the mixture, and this enables the matching of shock layer temperatures at lower flow velocities [25]. CH_4 was not included in the considered test gas compositions, similarly to the computational investigation in [4], as the concentration of CH_4 is not expected to increase significantly until well below the Uranus peak heating point altitude [26].

Table 1. Uranus Peak Heating X2 Operating Conditions

	UPH1	**UPH2**	**UPH3**
Driver fill gas (by volume)	77.2 kPa 100%He	77.2 kPa 100%He	77.2 kPa 100%He
Primary diaphragm	2.5mm steel	2.5mm steel	2.5mm steel
Shock tube gas (by volume)	2600 Pa 40%He/60%H2	8400 Pa 50%He/50%H2	23000 Pa 60%He/40%H2
Secondary Diaphragm	2-micron mylar	2-micron mylar	5-micron mylar
Acceleration Tube	1.5 Pa	5.6 Pa	16 Pa

Overall, five usable shots were obtained each for UPH1 and UPH2, with four usable shots for UPH3. The experimental shock speeds vs Pitot3 predictions for each condition are shown in Fig. 4, where VS1 and VS2 correspond to the shock tube and acceleration speeds, respectively. There is an inverse correlation between the amount of helium diluent in the test gas composition and the resulting shock

speeds throughout the test, as expected, with the lowest helium percentage condition "UPH1" exhibiting the highest shock speeds throughout. Furthermore, it can be seen that the VS1 shock speeds exhibit smaller variation across shots relative to the VS2 shock speeds. This is due to the fill pressure of the acceleration tube being typically in the order of 1-20 Pa and therefore more sensitive to variations in tunnel fill pressures across repeated shots [24]. The majority of shots were within 5% of the predicted VS1 and VS2 shock speeds by Pitot3, with the exception of one outlier each for UPH2 and UPH3. The outliers may be due to either overfilling of the shock tube or underfilling of the acceleration tube prior to the shot.

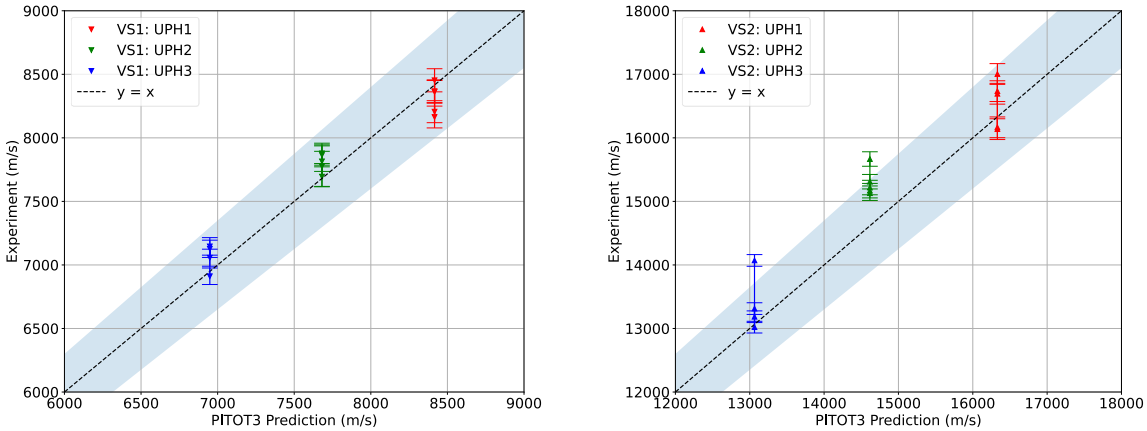

Fig. 4 Shock Tube (left) and Acceleration Tube (right) Shock Speeds

The pitot pressure profiles for each shot across the three conditions tested are shown in Fig. 5. It was found that the pitot pressures for each shot are on average higher than that predicted by Pitot3, as can be seen in Table 3. This may be due to the boundary layer development in the nozzle, whereby the effective area ratio of the nozzle in the experiments becomes smaller than the geometric area ratio of 5.64, which is the value initially used by PITOT3, and this has been shown to have a large effect on the nozzle exit flow density and pressure [24]. The average area ratios required for conditions UPH1 and UPH2, to enable PITOT3 to match the experimentally measured mean pressures were 2.6 +/- 0.05 and 4.05 +/- 0.57, respectively. In terms of shot-to-shot repeatability, UPH1 can be seen to have the lowest shot to shot variation in absolute pressure throughout the core flow, and UPH3 is shown to have the highest, in contrast to the trends shown in the shock speeds.

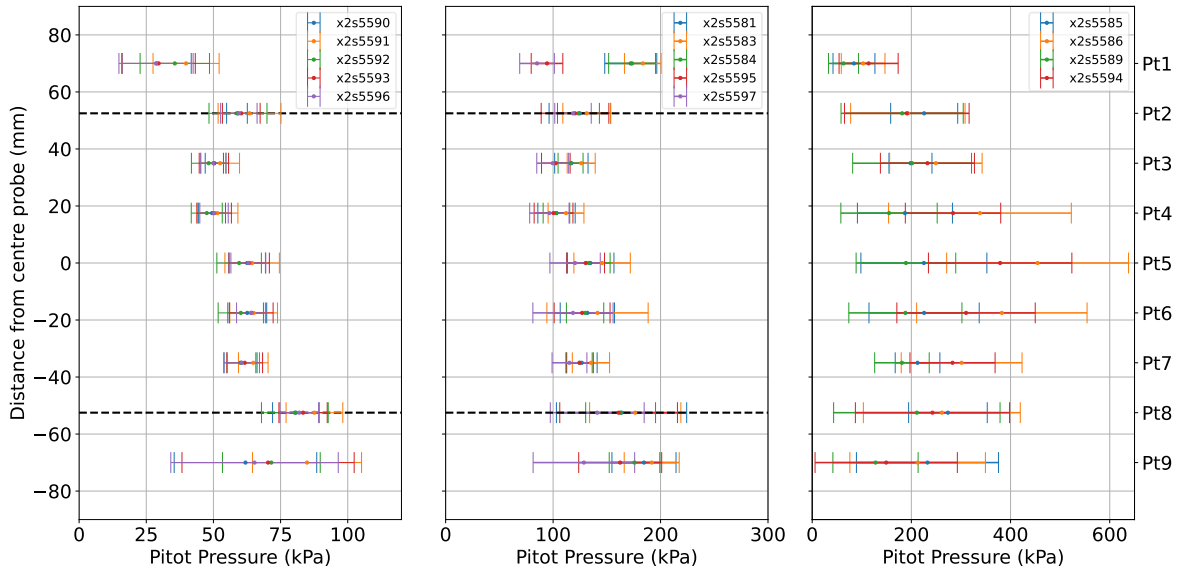

Fig. 5 Pitot Pressure Profiles for Uranus Peak Heating Test Conditions

(UPH1: left, UPH2: centre, UPH3: right)

Matthew Uren[1], Yu Liu[1], Chris James[3], Richard Morgan[4]

Inspection of how the test-time-averaged pressure varies for each probe for the three test conditions yields insights as to how big the core flow region might be. For UPH1, the uncertainty in Pitot pressure is significantly less for the central five probes, whereas for probes Pt2 and Pt8, the uncertainty is higher, and the absolute pressure readings start to diverge from the mean. Additionally, there is a large drop in measured pressure for the most outer probes Pt1 and Pt9. Assuming a core flow size of 100 mm for UPH1 results in a mean pressure of 61.5 kPa +/- 1.8 kPa. The uncertainty bars for the UPH2 pressure measurements vary more across each probe and are larger than those for UPH1. However, the absolute pressures diverge over Pt1, and Pt8 and Pt9 measured higher absolute pressures relative to the central five probes. Similarly to UPH1, assuming the core flow size is 100 mm results in a mean pressure of 120.8 kPa +/- 7.8 kPa. UPH3 returned the worst shot to shot repeatability in terms of absolute pressures across each probe, as well as large uncertainties for each pressure measurement. This is particularly pronounced for Pt4-Pt6, which contrasts with what should be expected for a steady test flow. Furthermore, the assessment of the Pitot pressure traces for UPH3 showed no overlap in steady pressure data, unlike that of the shots in Fig. 3. As a result, further analysis on the suitability of these conditions for future experiments was constrained to UPH1 and UPH2 exclusively.

The average freestream and post shock flow properties for UPH1 and UPH2, calculated by PITOT3 and derived from the experimental shock speed and pressure measurements, are shown in Table 2 and Table 3, respectively. The predictions calculated by PITOT3 in theoretical mode are also shown in comparison. The freestream flow properties are higher than initially predicted, however they are all within the same order of magnitude, with standard deviations generally less than 10% of the average value. The freestream velocity is well matched for UPH1 and less so for UPH2 at roughly 5% higher than the theoretical prediction.

Table 2. UPH Test Conditions Freestream Properties

	Target	**Theoretical**			**Experimental**	
Parameter	**Palmer** [4]	**UPH1**	**UPH2**	**UPH3**	**UPH1**	**UPH2**
Pressure (Pa)	588	191	526	1055	420 +/- 20	650 +/- 60
Temperature (K)	66.36	504	409	315	635 +/- 15	450 +/- 10
Density (kg/m^3)	2.47E-03	1.28E-04	4.6+5E-04	1.29E-03	2.3E-04 +/- 1.45E-05	5.2E-04 +/- 4.3E-05
Velocity (m/s)	19716	16691	14936	13335	16600 +/- 450	15550 +/- 200

The post shock parameters vary more across the two conditions, as can be seen in Table 3. The post shock equilibrium pressure, density, and temperatures are higher than that initially predicted by PITOT3. This is unsurprising due to the higher acceleration tube shock speeds shown in Fig. 4 which results in a higher enthalpy test flow, and the possible influence of the reduction in nozzle area ratio. The standard deviations on all flow parameters are within 10% showing reasonable repeatability across shots. Using the overlapping steady time method described in Section 2, the average steady test times for UPH1 and UPH2 were 50 μs and 35 μs, respectively. The higher steady test time for UPH1 is in contrast to what would be expected, as it has a higher freestream test flow velocity than UPH1. However, the mean pressure profiles in Fig. 5 appears to suggest that the higher pressure fill conditions result in a more unsteady shock layer, although, this should be investigated further. The shock layer temperatures in the order of 4000-5000 K also result in a highly dissociated shock layer as can be seen by the high percentages of atomic versus molecular hydrogen. Furthermore, to highlight the potential severity of heat release by atomic recombination, the fraction of the total enthalpy of the flow contained within dissociation is presented. For all conditions, over half of the total flow enthalpy is consumed in dissociation and stored as chemical potential energy. The importance of the catalytic behaviour of carbon-based heat shields in atomic hydrogen dominated shock layers is clear, as the catalytic recombination efficiency could have a large influence on the design and performance of the thermal protection system for ice giant planetary entry.

Table 3. UPH Test Conditions Equilibrium Post Shock Properties

	Target	Theoretical			Experimental	
Parameter	**Palmer** [4]	**UPH1**	**UPH2**	**UPH3**	**UPH1**	**UPH2**
Pressure (Pa)	884270	32975	94718	207290	58000 +/- 2000	115000 +/- 7000
Temperature (K)	4947	4560	4600	4674	4800 +/- 300	5200 +/- 200
Density (kg/m^3)	3.1E-02	1.55E-03	5.1E-03	1.26E-02	2.6E-03 +/- 2.4E-04	5.4E-03 +/- 5.5E-04
Pitot pressure (kPa)	-	34.5	99.5	219.3	61.5 +/- 1.8	120.8 +/- 7.8
Total enthalpy (MJ/kg)	191.7	141.2	112.5	89.04	143 +/- 6	122 +/- 3
H_2 mole fraction (%)	14.1	1.3	2.4	3.0	1.5 +/- 1.0	0.85 +/- 0.35
H mole fraction (%)	76.6	73.4	63.4	52.8	73.1 +/- 1.3	65.5 +/- 0.45
He mole fraction (%)	9.25	25.3	34.1	44.2	25.4 +/- 0.27	33.6 +/- 0.14
H_2 Dissociation fraction (%)	73.1	96.6	92.9	89.8	98.0 +/- 1.4	98.7 +/- 0.5
Total enthalpy in dissociation (%)	60.8	63.4	59.5	54.4	62.0 +/- 1.1	57.5 +/- 0.9

Spectroscopic measurements of the flow over a single probe are shown below in Fig. 6 for conditions UPH1 and UPH2, from the 200 nm – 1000 nm small fibre-coupled spectrometer. The spectrometer was triggered 50 µs after initial flow arrival and was exposed to the test flow for a duration of 50 µs for the majority of shots, with a minority at an exposure of 100 µs. These spectral measurements were collected to gain an insight as to what species would radiate for the candidate Uranus peak heating test conditions. The lower pressure condition UPH1 results in much less flow contamination than UPH2, with the clear distinction being the absence of the oxygen and nitrogen lines from 700 nm to 900 nm in the UPH1 shots. The oxygen and nitrogen lines in the UPH2 shots indicate either a potential leak into the shock tube during the fill process or the spectrometer capture time included part of the accelerator gas. The latter may be possible due to these signals being isolated to UPH2, however, this should be investigated further. In both conditions, the Na and H-alpha lines at 589 nm and 656 nm, respectively, were of comparable signal strength. Iron and carbon contamination can be seen around 380 nm – 390 nm for both test conditions and it is likely these originate from the facility itself, as has been observed also by [27], [28].

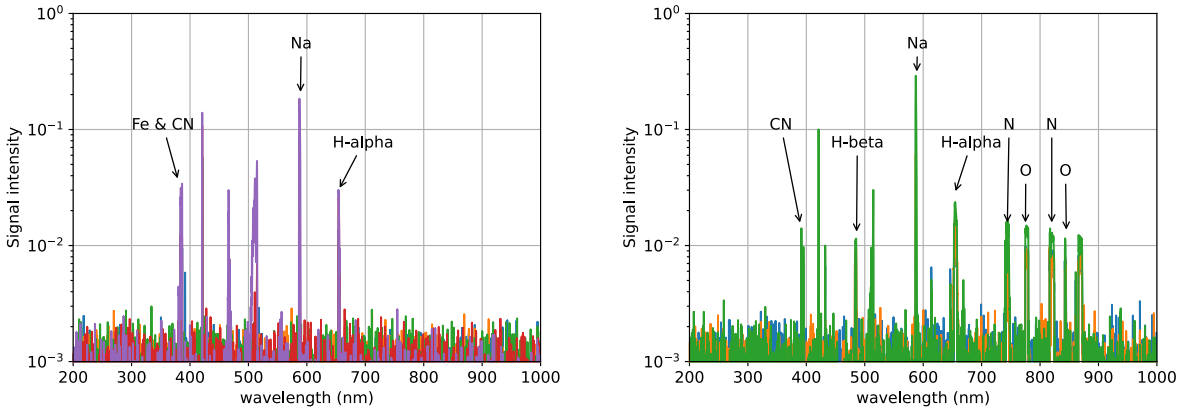

Fig. 6 Small fibre-coupled spectrometer results for UPH1 (left) and UPH2 (right)

4. Thermal Analysis

The test conditions presented have been generated to study surface heat flux over a test model in an ice giant representative flow field, and therefore to measure heat flux using infrared thermography, there must be a suitable rise in surface temperature during the test time. Furthermore, the predicted heat flux of each test case should be matched to the expected trajectory point of the real flight case, if the model material response is of interest. An initial thermal analysis of these candidate peak heating conditions has been performed using three stagnation-point heat flux correlations in combination with the semi-infinite 1D heat conduction analysis described in [29]. The stagnation-point heat flux correlations employed are the generic Sutton & Graves correlation [30], a modified Sutton & Graves correlation presented in the ESA CDF Ice Giant Report [2], and a more recent correlation from Carroll & Brandis [31], and these are given by equations 4.1, 4.2, and 4.3, respectively.

$$\dot{q} = K\sqrt{\frac{p_{stag}}{R_N}}(h_s - h_w) = K\sqrt{\frac{\rho}{R_N}}{V_\infty}^3 \tag{4.1}$$

$$\dot{q} = 9.08\sqrt{\frac{1}{2R_N}}\rho^{0.419778}\left(\frac{V_\infty}{1000}\right)^{2.67892} \tag{4.2}$$

$$\dot{q}\sqrt{\frac{R_N}{p_{stag}}} = c_1\left(\left(\frac{V_\infty}{45000}\right)^2 + d_1\left(\frac{V_\infty}{45000}\right)\right)R_N^{e_1}\left(\frac{\log_{10}\rho}{-5}\right)^{f_1} \tag{4.3}$$

Where c_1, d_1, e_1, and f_1 in equation 4.3 are coefficients dependent on the total enthalpy of the flow. The stagnation-point heat flux using each correlation has been calculated for test conditions UPH1 and UPH2 over a range of nose radii typical of models that have been used in the X2 expansion tube, and these range from 10 mm to 45 mm. These are generally chosen according to binary scaling laws and the available core flow size of the test flow; however, the model must also not be so large as to prevent a stable shock layer from developing over it during the steady flow test time. For that reason, a conservative core flow limit of 80 mm has been chosen and this is represented by the dashed black line. The resultant stagnation-point heat flux and expected surface temperature rise for UPH1 and UPH2 is shown in Fig. 7, on the left y-axis and right y-axis, respectively. For the 1-D semi-infinite heating calculations, graphite ET10 was chosen as a carbon-based test sample representative of the carbon phenolic heat shields typically used in high enthalpy planetary entries.

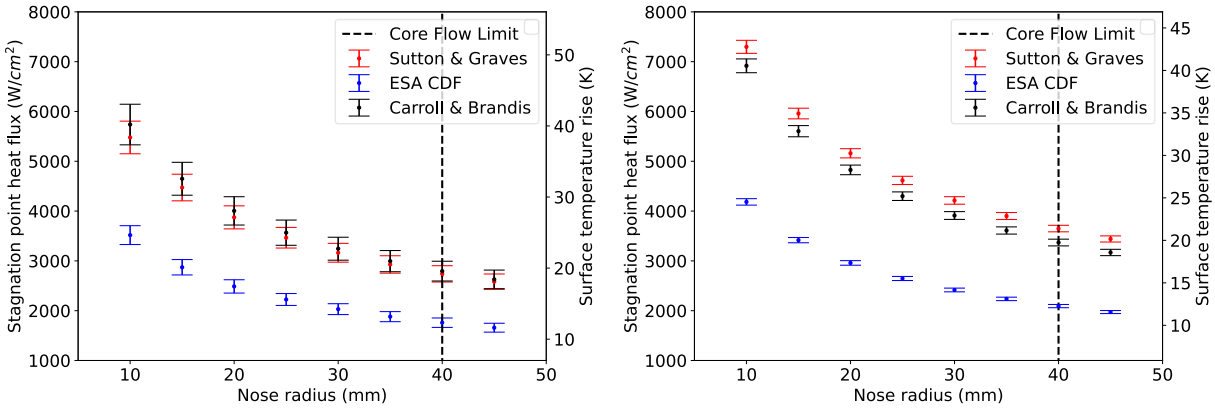

Fig. 7 Stagnation-point heat flux and surface temperature rise for UPH1 (left) and UPH2 (right)

The surface temperature rise for conditions UPH1 and UPH2 range from 10 K to 45 K, and the stagnation-point heat flux ranges from approximately 1500 W/cm^2 to 8000 W/cm^2, dependent on the model nose radius and correlation used. For comparison, the equilibrium peak heating trajectory point heat flux presented in [4] is 1942 W/cm^2. The range of heat fluxes calculated here is higher than

that, however, stagnation-point heat flux correlations are generally derived with the conservative assumption that the surface is fully catalytic. This refers to the heat flux due to reclamation of chemical potential energy by recombination of dissociated species on the material surface, and this can be a large contributor to the total heat flux to a vehicle. Although the test conditions designed return higher predicted heat fluxes than the target condition from [4], they do lie within the ice giant shallow and steep entry heat flux regions presented in [32].

For all correlations employed, the heat flux inversely correlates with the square root of nose-radius, and this can be attributed to the influence of the model nose radius on the shock stand-off distance. If the shock front is located further away from the vehicle or model, this results in a reduced temperature gradient, therefore decreasing the rate of thermal energy transfer from the hot shock layer to the surface. The analysis shows good agreement between the original Sutton & Graves correlation and the correlation developed by Carroll and Brandis. However, the correlation presented in the ESA CDF Ice Giant report returns heat fluxes a factor of 1.5-2 lower than the other correlations. It is unclear as to why this discrepancy exists and the background material regarding the derivation of this correlation is not publicly available. Nevertheless, these results offer an upper and lower bound for the stagnation-point heat flux and surface temperature rise for the two Uranus peak heating conditions investigated in the X2 expansion tube.

5. Implications for future work

The successful application of IR thermography for these conditions requires a suitable rise in surface temperature with a steady test time long enough to capture thermographic images. Another key requirement is the selection of a suitable wavelength window where contamination from the X2 facility will not obscure IR measurements of the surface grey body radiation. In previous experiments by Liu in the X2 expansion tube, H-alpha (656 nm) and H-beta (486 nm) were the primary radiators, followed by Al and Al ions due to the usage of an aluminium secondary diaphragm [13]. Although, these were seen within a wavelength range below that which encompasses the wavelength region of the camera used in previous X2 IR thermography experiments. The present experiments were conducted with a mylar secondary diaphragm which has been shown by [33] to result in lower flow contamination than an aluminium secondary diaphragm. However, they reported a base level of contamination for the Mylar test case after a comparison between shots with radiating air and non-radiating helium test gas. NEQAIR was also used by [33] to obtain an optical sub-window for a high enthalpy Apollo return condition between 2000 and 2500 nm for IR thermography, with a minimum pre-heated model surface temperature of 1400 K. The shock layer radiation for a Uranus peak heating point flow is expected to be negligible due to the near absence of CH_4, which has been highlighted by [17] to contribute to faster ionization and therefore flow radiation. On that basis, it could be assumed rather conservatively that a minimum optical sub-window between 2000 and 2500 nm is therefore possible with the current Uranus peak heating test conditions.

The steady test time of 50 μs and 35 μs for UPH1 and UPH2, respectively, could also be a limiting factor on obtaining detailed time-resolved thermographic measurements. Previous work on X2 in using an IRC806HS IR camera [34] with a wavelength range of 1-5 μm stated it was possible to get an image every 46.5 μs by sub-windowing the image to a window size of 8 x 320 pixels, although, this resulted in only a narrow strip of the test model being available to take thermographic measurements of. However, a similar investigation by [20] showed the benefits of using a single discrete point IR sensor for highly time-resolved validation of the IR camera measurements. Additionally, the surface temperature rise predictions in Section 4 are of a similar order of magnitude to the experimentally measured temperature rises between frames in [20,34]. Therefore, if a suitable wavelength window is found from future spectral measurements, the signal change with time of the surface radiation should be capturable by the IR camera available. The possibility of using visible to near-IR thermography for a Uranus entry condition has also been computationally investigated by [35], where considerable wavelength windows for a pre-heated model at a minimum surface temperature of 800 – 1000 K were identified. The successful implementation of this method would allow highly time-resolved data at a 1 MHz frame rate to be captured, thereby allowing detailed surface temperature measurements to be made over the steady flow test time. A comprehensive spectroscopy investigation of the conditions presented here would give credibility to this by experimental validation.

6. Conclusions

Three new test conditions representative of a Uranus entry peak heating trajectory point have been investigated in the X2 expansion tube using helium test-gas substitution. A Pitot rake array was used in combination with optical measurements to characterise the new test conditions by identifying steady test time, core flow size, and freestream and equilibrium post shock flow properties. Out of the three test conditions, two were deemed appropriate candidate test conditions for future investigations of surface heat flux. The lowest fill-pressure condition, UPH1, showed the highest potential due to low levels of contamination, a higher steady test time, and post shock flow parameters closer to the target peak heating condition. Thermal analysis of the chosen flow conditions over a range of potential test model sizes returned stagnation-point heat flux predictions consistent with those in the literature and surface temperature rises of a graphite model comparable to previous IR thermography experiments in the X2 expansion tube. The importance of selecting a suitable waveband for thermographic measurements was highlighted, primarily due to the necessity in obtaining a sufficient signal-noise ratio for the test model surface over shock layer radiation or residual contamination from the test facility. Future experiments aiming to measure heat flux optically for an ice giant entry representative test flow must ensure appropriate temporal and spatial resolution on the test model, and this is also dependent on the camera system and target waveband chosen. To conclude, following the characterization of these new test conditions and accompanying thermal analysis, future efforts will focus on developing a series of experiments to successfully perform IR thermography using the test conditions presented here, in support of thermal protection system development and computational validation for future exploration missions of the ice giants.

7. Acknowledgements

This research was supported by the Australian Research Council through Project DP220103330. Dr. Christopher James was funded by the Australian Research Council through the Discovery Early Career Researcher Award number DE210101072 when this work was performed. Matthew Uren is a recipient of an Australian Government Research Training Program Scholarship. The first author is also pleased to acknowledge the contribution of the IMechE Whitworth Senior Scholarship Award in supporting this research. The authors would like to thank Mr. Neil Duncan and Mr. Keith Hitchcock for technical support, as well as the operators for X2 past and present for keeping the facility running well.

8. References

[1] M. Hofstdater, A. Simon, K. Reh, J. Elliott, C. Niebur, and L. Colangeli, "Ice Giants Pre-Decadal Survey Mission Study Report," 2017.

[2] ESA, S. Bayon, and M. Bandecchi, "CDF Study Report: A Mission to the Ice Giants – Neptune and Uranus," 2019.

[3] B. Laub and E. Venkatapathy, "Thermal protection system technology and facility needs for demanding future planetary missions," 2004. [Online]. Available: https://www.researchgate.net/publication/234437942

[4] G. Palmer, D. Prabhu, and B. A. Cruden, "Aeroheating uncertainties in uranus and saturn entries by the Monte Carlo method," in *Journal of Spacecraft and Rockets*, American Institute of Aeronautics and Astronautics Inc., 2014, pp. 801–814. doi: 10.2514/1.A32768.

[5] Y. Liu, "Non-equilibrium Radiation in Simulated Giant Planet Entries," PhD Thesis, The University of Queensland, 2021.

[6] J. Coelho and M. Lino da Silva, "Aerothermodynamic analysis of Neptune ballistic entry and aerocapture flows," *Advances in Space Research*, vol. 71, no. 8, pp. 3408–3432, Apr. 2023, doi: 10.1016/j.asr.2022.12.024.

[7] C. E. Higgins, "Aerothermodynamics of the Gas Giants," PhD Thesis, The University of Queensland, 2004.

[8] G. R. Inger, C. Higgins, and R. Morgan, "Shock standoff on hypersonic blunt bodies in nonequilibrium gas flows," *J Thermophys Heat Trans*, vol. 16, no. 2, pp. 245–250, 2002, doi: 10.2514/2.6674.

[9] H. Herbrig, "Investigation of Hypervelocity Flows with Large Amounts of Ionisation and Dissociation in a H2/Ne Test Gas," PhD Thesis, University of Stuttgart, 1999.

[10] C. M. James, D. E. Gildfind, R. G. Morgan, S. W. Lewis, E. J. Fahy, and T. J. McIntyre, "On the current limits of simulating gas giant entry flows in an expansion tube," in *20th AIAA International Space Planes and Hypersonic Systems and Technologies Conference, 2015*, AIAA American Institute of Aeronautics and Astronautics, 2015. doi: 10.2514/6.2015-3501.

[11] C. M. James, D. E. Gildfind, R. G. Morgan, S. W. Lewis, and T. J. McIntyre, "Simulating Gas Giant Atmospheric Entry Using Helium and Neon Test Gas Substitutions," *J Spacecr Rockets*, vol. 56, no. 3, pp. 725–743, May 2019, doi: 10.2514/1.A34282.

[12] C. M. James, Y. Liu, and R. G. Morgan, "Experimentally Simulating Giant Planet Entry in an Expansion Tube," in *AIAA AVIATION 2020 FORUM*, American Institute of Aeronautics and Astronautics Inc, AIAA, 2020, pp. 656–671. doi: 10.2514/1.A34457.

[13] Y. Liu, C. M. James, R. G. Morgan, and T. J. McIntyre, "Experimental validation of a test gas substitution for simulating non-equilibrium giant planet entry conditions in impulse facilities," *Exp Fluids*, vol. 61, no. 9, Sep. 2020, doi: 10.1007/s00348-020-03032-3.

[14] Y. Liu, C. M. James, R. G. Morgan, P. A. Jacobs, R. Gollan, and T. J. Mcintyre, "Electron number density measurements in a Saturn entry condition."

[15] J. Steer *et al.*, "Shock Radiation Tests for Ice Giant Entry Probes Including CH 4 in the T6 Free-Piston Driven Wind Tunnel," in *AIAA SCITECH 2023 Forum*, doi: 10.2514/6.2023-1729.

[16] S. Loehle *et al.*, "Experimental Simulation of Gas Giant Entry in the PWK1 Arcjet Facility including CH4," in *AIAA Science and Technology Forum and Exposition, AIAA SciTech Forum 2022*, American Institute of Aeronautics and Astronautics Inc, AIAA, 2022. doi: 10.2514/6.2022-0264.

[17] B. A. Cruden and A. C. Tibère-Inglesse, "Impact of Trace CH_4 on Shock Layer Radiation in Outer Planet Entry," in *AIAA SCITECH 2024 Forum*, Reston, Virginia: American Institute of Aeronautics and Astronautics, Jan. 2024. doi: 10.2514/6.2024-2084.

[18] J. Steer *et al.*, "Experimental Study of a Galileo Sub-Scale Model at Ice Giant Entry Conditions in the T6 Free-Piston Driven Wind Tunnel," in *AIAA SCITECH 2023 Forum*, doi: 10.2514/6.2023-1339.

[19] T. G. Cullen *et al.*, "Infrared thermography on a biconic model in hypersonic expansion tube flows," in *AIAA Scitech 2021 Forum*, American Institute of Aeronautics and Astronautics Inc, AIAA, 2021, pp. 1–19. doi: 10.2514/6.2021-0873.

[20] R. Ramesh, R. G. Morgan, and D. J. Mee, "Heat Transfer Measurements in an Expansion Tube Using Infrared Thermography," *AIAA Journal*, vol. 60, no. 2, pp. 883–891, Feb. 2022, doi: 10.2514/1.J059919.

[21] D. E. Gildfind, R. G. Morgan, and P. A. Jacobs, "Expansion tubes in Australia," in *Experimental Methods of Shock Wave Research*, Springer International Publishing, 2016, pp. 399–431. doi: 10.1007/978-3-319-23745-9_13.

[22] F. Zander, R. G. Morgan, U. Sheikh, D. R. Buttsworth, and P. R. Teakle, "Hot-wall reentry testing in hypersonic impulse facilities," *AIAA Journal*, vol. 51, no. 2, pp. 476–484, Feb. 2013, doi: 10.2514/1.J051867.

[23] C. M. James, "Using a Simplified Canny Edge Detector to Detect Shock Arrival in Expansion Tubes and Shock Tunnels," Research Publishing Services, Feb. 2020, pp. 651–672. doi: 10.3850/978-981-11-2730-4_0031-cd.

[24] C. M. James, D. E. Gildfind, S. W. Lewis, R. G. Morgan, and F. Zander, "Implementation of a state-to-state analytical framework for the calculation of expansion tube flow properties," *Shock Waves*, vol. 28, no. 2, pp. 349–377, Mar. 2018, doi: 10.1007/s00193-017-0763-3.

[25] R. J. Stalker and B. P. Edwards, "Hypersonic blunt-body flows in hydrogen-neon mixtures," *J Spacecr Rockets*, vol. 35, no. 6, pp. 729–735, 1998, doi: 10.2514/2.3399.

[26] J. B. Scoggins, A. D. Hinkle, and E. Shellabarger, "Aeroheating Environment of Aerocapture Systems for Uranus Orbiters," in *AIAA SCITECH 2024 Forum*, Reston, Virginia: American Institute of Aeronautics and Astronautics, Jan. 2024. doi: 10.2514/6.2024-0951.

[27] C. M. James *et al.*, "Improved test time evaluation in an expansion tube," *Exp Fluids*, vol. 59, no. 5, May 2018, doi: 10.1007/s00348-018-2540-1.
[28] S. Lewis, "Hypervelocity Shock Layer Emission Spectroscopy with High Temperature Ablating Models," PhD Thesis, The University of Queensland.
[29] D. Schultz and T. Jones, "Heat-transfer Measurements in Short-duration Hypersonic Facilities," 1973.
[30] K. Sutton and R. A. Graves, "A GENERAL STAGNATION-POINT CONVECTIVE-HEATING EQUATION FOR ARBITRARY GAS MIXTURES."
[31] A. T. Carroll and A. M. Brandis, " Stagnation Point Convective Heating Correlations for Entry into H 2 /He Atmospheres ," American Institute of Aeronautics and Astronautics (AIAA), Jan. 2023. doi: 10.2514/6.2023-0208.
[32] E. Venkatapathy *et al.*, "Entry System Technology Readiness for Ice-Giant Probe Missions," *Space Sci Rev*, vol. 216, no. 2, Mar. 2020, doi: 10.1007/s11214-020-0638-2.
[33] T. G. Cullen, "Optically based heat flux measurements in radiating expansion tunnel flows," PhD Thesis, The University of Queensland.
[34] T. Cullen, C. James, R. Gollan, and R. Morgan, "Application of Infrared Thermography in an Expansion Tunnel."
[35] L. Alemany, C. M. James, and T. G. Cullen, "Investigation of Visible to Near-Infrared High-Speed Thermography for Atmospheric Reentry Testing," *Exp Fluids*, vol. 64, no. 12, 2023.